



THIS MANUSCRIPT HAS BEEN SUBMITTED TO THE JOURNAL OF GLACIOLOGY AND HAS NOT BEEN PEER-REVIEWED.

DAS to Discharge: Using Distributed Acoustic Sensing (DAS) to infer glacier runoff

Journal:	<i>Journal of Glaciology</i>
Manuscript ID	JOG-2024-0014
Manuscript Type:	Article
Date Submitted by the Author:	05-Feb-2024
Complete List of Authors:	Manos, John-Morgan; University of Washington, Earth and Space Sciences Gräff, Dominik; University of Washington, Earth and Space Sciences Martin, Eileen; Colorado School of Mines, Department of Geophysics Paitz, Patrick; Swiss Federal Institute for Forest Snow and Landscape Research WSL Walter, Fabian; Swiss Federal Institute for Forest Snow and Landscape Research WSL Fichtner, Andreas; ETH Zürich, Institut für Geophysik Lipovsky, Bradley; University of Washington College of the Environment, Department of Earth and Space Sciences
Keywords:	Glaciological instruments and methods, Glacier discharge, Melt - surface, Glacier hydrology, Seismology
Abstract:	Observations of glacier melt and runoff are of fundamental interest in the study of glaciers and their interactions with their environment. Considerable recent interest has developed around Distributed Acoustic Sensing (DAS), a sensing technique which utilizes Rayleigh backscatter in fiber optic cables to measure the seismo-acoustic wavefield in high spatial and temporal resolution. Here, we present data from a month-long, 9 km DAS deployment extending through the ablation and accumulation zones on Rhonegletscher, Switzerland, during the 2020 melt season. While testing several types of machine learning (ML) models, We establish a regression problem using the DAS data as the

	<p>dependent variable to predict the glacier discharge observed at a proglacial stream gauge. We also compare two models that only depend on meteorological station data. We find that the seismo-acoustic wavefield recorded by DAS can be utilized to infer proglacial discharge. Models using DAS data outperform both the models trained on meteorological data with mean absolute errors (MAE) of 0.64 m³/s, 2.25 m³/s, and 2.72 m³/s, respectively. This study demonstrates the ability of in situ glacier DAS to be used for quantifying proglacial discharge and points the way to a new approach to measuring glacier runoff.</p>

SCHOLARONE™
Manuscripts

DAS to Discharge: Using Distributed Acoustic Sensing (DAS) to infer glacier runoff

John-Morgan MANOS¹, Dominik GRÄFF¹, Eileen R. MARTIN², Patrick PAITZ³, Fabian
WALTER⁴, Andreas FICHTNER³, Bradley P. LIPOVSKY¹

¹*Department of Earth and Space Sciences, University of Washington, Seattle, WA, USA*

²*Department of Geophysics and Department of Applied Math and Statistics, Colorado School of Mines,
Golden, CO, USA*

³*ETH Zurich, Department of Earth Sciences, Institute of Geophysics, Zurich, Switzerland*

⁴*Swiss Federal Institute for Forest, Snow and Landscape Research WSL, Zürich, Switzerland*

Correspondence: John-Morgan Manos <jmanos@uw.edu>

ABSTRACT. Observations of glacier melt and runoff are of fundamental interest in the study of glaciers and their interactions with their environment. Considerable recent interest has developed around Distributed Acoustic Sensing (DAS), a sensing technique which utilizes Rayleigh backscatter in fiber optic cables to measure the seismo-acoustic wavefield in high spatial and temporal resolution. Here, we present data from a month-long, 9 km DAS deployment extending through the ablation and accumulation zones on Rhonegletscher, Switzerland, during the 2020 melt season. While testing several types of machine learning (ML) models, We establish a regression problem using the DAS data as the dependent variable to predict the glacier discharge observed at a proglacial stream gauge. We also compare two models that only depend on meteorological station data. We find that the seismo-acoustic wavefield recorded by DAS can be utilized to infer proglacial discharge. Models using DAS data outperform both the models trained on meteorological data with mean absolute errors (MAE) of 0.64 m³/s, 2.25 m³/s, and 2.72 m³/s, respectively. This study demonstrates the ability of *in situ* glacier DAS to be used for quantifying proglacial discharge and points the way to a new approach to

28 **measuring glacier runoff.**

29 INTRODUCTION

30 Glaciers are an important yet diminishing reservoir of freshwater for communities and ecosystems (Casassa
31 and others, 2009). In the European Alps, for example, modeled future trends indicate a large reduction or
32 disappearance of glaciers on decadal timescales due to climate change (Haeberli and others, 2007; Linsbauer
33 and others, 2013; Zekollari and others, 2019). Glacierized catchments provide a river discharge buffering
34 mechanism, particularly important during the dry season. This mechanism will likely be disrupted if
35 alpine glaciers continue to retreat and to disappear (Mark and Seltzer, 2003) with immediate effects on
36 the downstream ecology which is particularly susceptible to changes in glacier-sourced freshwater input
37 to proglacial streams (Cauvy-Fraunié and others, 2016). In addition, hydroelectric power production
38 is expected to decrease within the century as a substantial part of the current hydroelectric power is
39 produced by unsustainable glacier mass loss caused by the warming climate (Schaeffi and others, 2019).
40 As infrastructure grows and glaciers retreat, it will become increasingly important to measure glacier melt
41 runoff and accurately predict its contribution to the catchment's freshwater resources on seasonal and
42 diurnal timescales.

43 Glacier surface melt is the primary contributor to the mid latitude glacier hydrological system (Shreve,
44 1972). However, it remains difficult to observe the dominant processes that drive surface melt with sufficient
45 spatial and temporal resolution (Landmann, 2022). Conventional *in situ* methods for measuring glacier
46 surface ablation include ablation stakes (Pratap and others, 2015; Fountain and Vecchia, 1999; Landmann
47 and others, 2021) and the use of meteorological data to calculate energy fluxes that result in glacier surface
48 melt (Braithwaite, 1995; Hanna and others, 2005; Lenaerts and others, 2019). Although ablation stake
49 measurements and reconstruction from meteorological station data are foundational methods, they come
50 with the significant disadvantage of being labor intensive and therefore difficult to implement glacier-wide,
51 long-term studies. Satellite remote sensing, in contrast, offers the only feasible way to monitor glacial melt
52 at a global scale. A wide variety of remote sensing methods have been used to infer glacier surface melt
53 indirectly through observed changes in glacier elevation (Markus and others, 2017; Sutterley and others,
54 2018), mass (Wouters and others, 2008), or surface backscatter (Ridley, 1993; Trusel and others, 2013;
55 Bevan and others, 2018). Although satellite remote sensing may offer true global coverage, it oftentimes

56 lacks the spatial or temporal resolution required to resolve rapid, local variations in surface melt (Yang and
57 Smith, 2013; Yang and Li, 2014; Wille and others, 2019). More fundamentally, even when remote sensing
58 of glacier surface melt is able to attain a desired spatial and temporal resolution (Trusel and others, 2013;
59 Bevan and others, 2018; Sutterley and others, 2018), such platforms nevertheless benefit from –and in many
60 cases require– *in situ* observations for calibration and validation. Advances in satellite remote sensing of
61 glacier melt therefore motivate the need for improved *in situ* observations of glacier surface melt.

62 The familiar variety of sounds associated with flowing water attests to the ubiquity of flow-induced
63 acoustics. A correspondingly large number of previous studies have examined the seismo-acoustic wavefield
64 generated by water flow. Basic physical processes implicated in the generation of sound from flowing water
65 include wave breaking (Manasseh and others, 2006), hydraulic jump formation (Ronan and others, 2017),
66 low frequency fluid pulsing in conduits (Podolskiy, 2020), and the entrainment and collapse of air bubbles
67 in turbulent flows (Prosperetti, 1988; Morse and others, 2007). In terrestrial rivers, both discharge and
68 bedload transport contribute to the seismic wavefield (Burtin and others, 2008, 2011; Gimbert and others,
69 2016; Roth and others, 2016, 2017; Cook and others, 2018), as do roughness elements such as boulders (and
70 resulting rapids) and engineered blocks and weirs (Schmandt and others, 2013; Osborne and others, 2021,
71 2022). In glaciers, flow in subglacial conduits is constrained by conduit size with an observable impact on
72 the seismic wavefield (Bartholomaus and others, 2015; Nanni and others, 2020).

73 Here, we utilize Distributed Acoustic Sensing (DAS) to record the seismo-acoustic wavefield originating
74 from turbulent supraglacial water flow. The sensing component of DAS is a single mode optical fiber
75 cable deployed on the surface of the glacier. The basic measurement principle of DAS is that the phase
76 shift of Rayleigh-backscattered light in an optical fiber is used to infer the fiber axial strain rate with
77 spatial resolution on the order of several tens of centimeters and at frequencies, dependent on cable length,
78 of millihertz to several kilohertz (Shatalin and others, 2021), therefore enabling observation of seismo-
79 acoustic wavefields (Lindsey and Martin, 2021; Douglass and others, 2023). Fluid flow velocities within
80 pipes have been estimated using regression of DAS data (Vahabi and others, 2020; Titov and others, 2022).
81 Several studies have previously described glacier surface (Walter and others, 2020; Hudson and others,
82 2021) and borehole DAS deployments (Booth and others, 2023) for investigating the en- and subglacial
83 environment. Here, we leverage DAS observations from a 9-km long optical fiber deployed along the flow
84 line of an alpine glacier to examine the relationship between glacier melt and the *in situ* glacier surface
85 seismo-acoustic wavefield.

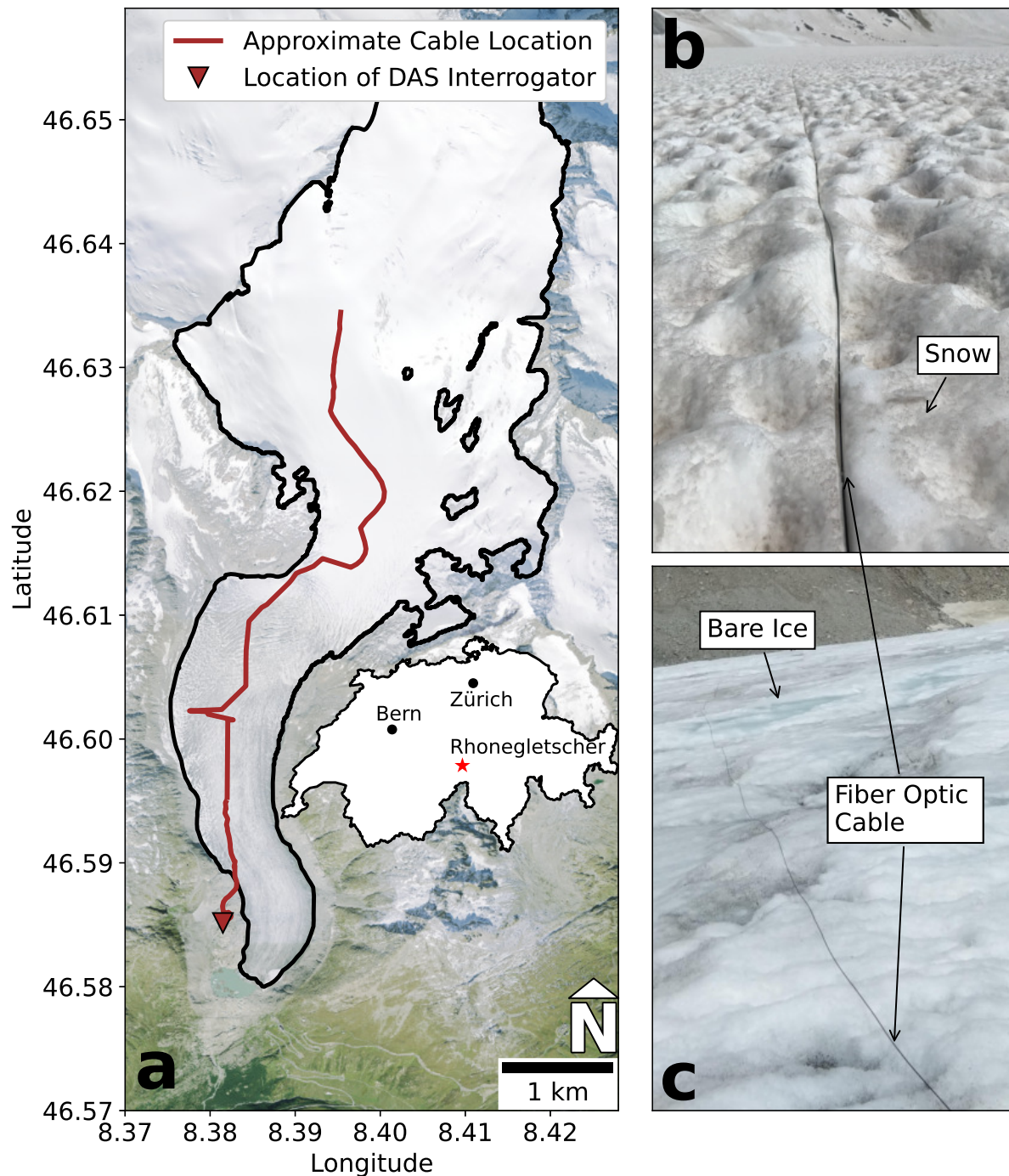


Fig. 1. a) Map of the study site. Approximate path of the fiber optic cable deployment and location of the Distributed Acoustic Sensing (DAS) interrogator including outline of Rhonegletscher (Consortium, 2005). Orthophoto provided from the Swiss Federal Office of Topography. b) Photo of the glacier surface and deployed cable in the accumulation zone (credit: Malgorzata Chmiel), consisting mostly of firn at the time of deployment (July 2020). c) Photo of the glacier surface and deployed cable in the ablation zone (credit: Sara Klaasen), consisting primarily of bare ice with areas of crevassing, meltwater surface streams, meltwater pools and glacier moulins.

86 FIELD SITE AND DATA

87 Rhonegletscher

88 Our measurements were conducted at Rhonegletscher, a temperate mountain glacier located in the central
89 Swiss Alps, in the summer of 2020 (Fig. 1a). The glacier covers a total area of 15.5 km² and ranges from
90 3600 m above sea level (a.s.l.) to 2200 m a.s.l. at its terminus with a length of about 8 km (GLAMOS and
91 others, 2020). During the field study, the surface of Rhonegletscher in the accumulation zone primarily
92 consisted of firn (Fig. 1b). The ablation zone was characterized by bare ice, crevasses, and distributed
93 supraglacial meltwater streams (Fig. 1c).

94 Distributed Acoustic Sensing (DAS) Deployment

95 A Silixa iDASTM interrogator was deployed in a tent west of the terminus of Rhonegletscher from July 4,
96 2020 to August 4, 2020. A 9 km single mode fiber optic cable was laid out on the surface of the glacier
97 approximately along the glacier flow line spanning across ablation and accumulation zones. During the
98 first portion of the experiment, interrogator recording settings such as channel spacing and sampling rate
99 were varied for instrument and sensitivity testing. Starting on July 13, settings remained constant for the
100 remainder of the experiment. To avoid complexities with different instrument settings, in this study we
101 only use the data from July 13 to August 4, 2020. During this time data was recorded continuously at 1 kHz
102 sampling frequency, 4 m channel spacing, and 10 m gauge length over 2496 channels. At this sampling
103 frequency, cable length, and gauge length, the iDASTM is sensitive to 2 picostrain per square root Hertz.
104 The last 188 channels contain instrument noise only, because the actual fiber optic cable length was shorter
105 than the length set in the interrogator settings. Thus, we only use the first 2308 channels for our analysis.
106 For most of our analysis, we high-pass filtered the data above 50 Hz. In later analysis, we investigate the
107 unfiltered DAS data to determine the influence of the broad band spectrum on discharge prediction. The
108 high-pass filter also mitigates the effects of thermal expansion with a diurnal period (Klaasen and others,
109 2021), shading from transient and local cloud cover, and from other anthropogenic sources (Huynh and
110 others, 2022) such as nearby hydropower production causing narrow-banded seismic energy at 16.7 Hz and
111 50 Hz. For each channel, we calculated the root mean square (RMS) of the fiber strain-rate for each 30 s
112 window of each channel in the DAS data (Fig. 2a).

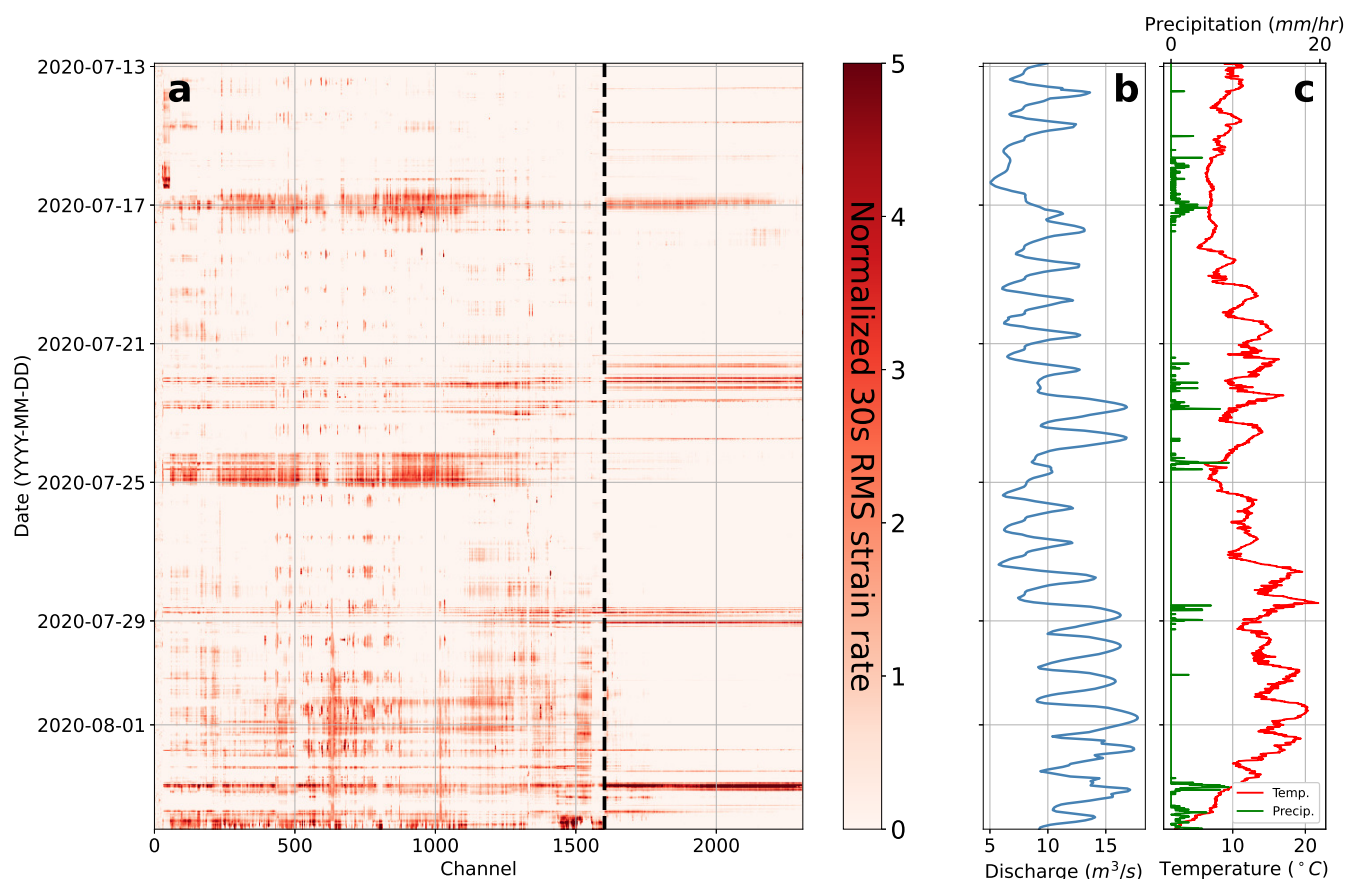


Fig. 2. a) DAS time series over analysis period. Data are highpass filtered above 50 Hz and normalized to peak RMS strain rate over all channels per time step. Low channel numbers are located closest to the terminus down-glacier (i.e. closer to the interrogator) and higher channel numbers are located progressively up glacier according to the plotted cable layout in Figure 1a. The dashed line denotes roughly the transition from the ablation zone down glacier and the accumulation zone up glacier. b) Rhône river discharge recorded about 3 km downstream of the proglacial lake. During the final two days of the experiment, a standing wave formed in the proglacial stream in the location of the discharge measurement resulting in the three crest pattern that is evident. c) Hourly temperature and precipitation data from 10 min recordings at Grimsel Hospitz meteo station (Swiss Federal Office of Meteorology and Climatology MeteoSwiss)

113 **Discharge measurements**

114 During summer, meltwater from Rhonegletscher is the primary contributor to the highest reaches of the
115 Rhône river near Oberwald, Switzerland. A radar-based discharge gauge (Swiss Federal Office for the
116 Environment, station ID number 2268) located in Gletsch about 3 km downstream of Rhonegletscher's
117 proglacial lake recorded hourly averaged discharge of the Rhône river throughout the duration of DAS
118 data collection. Discharge data (Fig. 2b) were linearly interpolated to 30 s to match the 30-second RMS
119 time steps calculated from the raw DAS data.

120 **Meteorological measurements**

121 We used meteorological data from the station Grimsel Hospiz (Swiss Federal Office of Meteorology and
122 Climatology MeteoSwiss) located 5-8 km southwest of Rhonegletscher behind a mountain ridge. Temper-
123 ature data were collected at 10 min intervals and precipitation data were recorded as the sum over the 10
124 min period (Fig. 2c).

125 **MACHINE LEARNING MODELS**

126 **Architectures: Linear, Neural Network, Long Short Term Memory**

127 In order to quantify the relationship between glacier melt and the recorded glacier surface seismo-acoustic
128 wavefield, we employ three separate machine learning models using Keras TensorFlow (Martín Abadi and
129 others, 2015) and assess their relative performance. We first implement a linear model with a single dense
130 layer with linear activation. This model mostly serves as a baseline point of comparison with two more
131 flexible models. Second, we implement a Neural Network (NN) model with two dense layers containing 32
132 units and a rectified linear unit (ReLU) activation function each, a flattening layer, and a dense layer with
133 one unit. Finally, we implement a Long Short-Term Memory (LSTM) model with a single LSTM layer
134 containing 32 units and a dense layer with one unit. The features (independent variables) in our analysis
135 consist of the multivariate time series of DAS strain rate data. The labels (dependent variables) in our
136 analysis consist of the measured discharge values from the downstream discharge gauge. These models are
137 each associated with learning rate, batch size, and data input window size hyperparameters; we choose
138 these hyperparameters based on the results of 90 experiments per model (see Figure S1). As a result of the
139 analysis, we choose a learning rate of 0.001, a batch size of 32 feature-target pairs, a window size of 200

140 time steps as these parameters produced stable and robust results. The Supplemental Information further
 141 describes hyperparameter tuning.

142 **Cross-validation scheme**

143 Previous studies of changes in supraglacial hydrology through space and time (Nicholson and others, 2021,
 144 e.g.) demonstrate that the surfaces of glaciers are inherently non-stationary over the timescale of several
 145 weeks during the melt season. Supraglacial stream geometry changes throughout the melt season and
 146 responds to change in water flow (Germain and Moorman, 2019). For this reason, we randomly shuffled
 147 the time series windows used for inputs prior to data separation into training, validation, and test sets.
 148 We therefore ensure that all possible glacier surface melt regimes occurring during the observation period
 149 are captured in the model training data set. In addition to shuffling, we use standard cross-validation
 150 (CV) techniques (Bishop and Nasrabadi, 2006, Chapter 14.2) wherein we perform 100 model trainings,
 151 each with a uniquely seeded test/training split. CV allows us to quantify model sensitivity to input data
 152 and estimate the non-stationary effect of the glacier surface on model performance.

153 **Meteo-LSTM model**

154 We consider an intermediate complexity, “Meteo-LSTM” model that uses an LSTM model architecture
 155 with temperature and precipitation data as features and discharge as labels. The goal of this model is to
 156 understand the impact of model complexity versus the underlying usefulness of different datasets by testing
 157 a model which has similar complexity to the DAS-LSTM model but only relies on the meteo station data.

158 **Positive degree-day (PDD) model**

159 Positive degree-day models are widely used to infer glacier melt from limited meteorological observations
 160 (Braithwaite, 1984). We implement a PDD model following Hock (Hock, 2005). We carry out a minimiza-
 161 tion analysis to select the melt rate factor and lapse rate value that resulted in the lowest absolute error
 162 in discharge. Temperatures as collected at Grimsel Hospiz were corrected over elevation bands of 100 m.
 163 Then the discharge prediction at each elevation band was summed to get the final predicted discharge,

$$D = \sum_{z=2.3 \text{ km}}^{3.6 \text{ km}} \begin{cases} \{(T + \gamma(z - z_0)) f + P\} A & T > 0 \\ PA & T \leq 0 \end{cases} \quad (1)$$

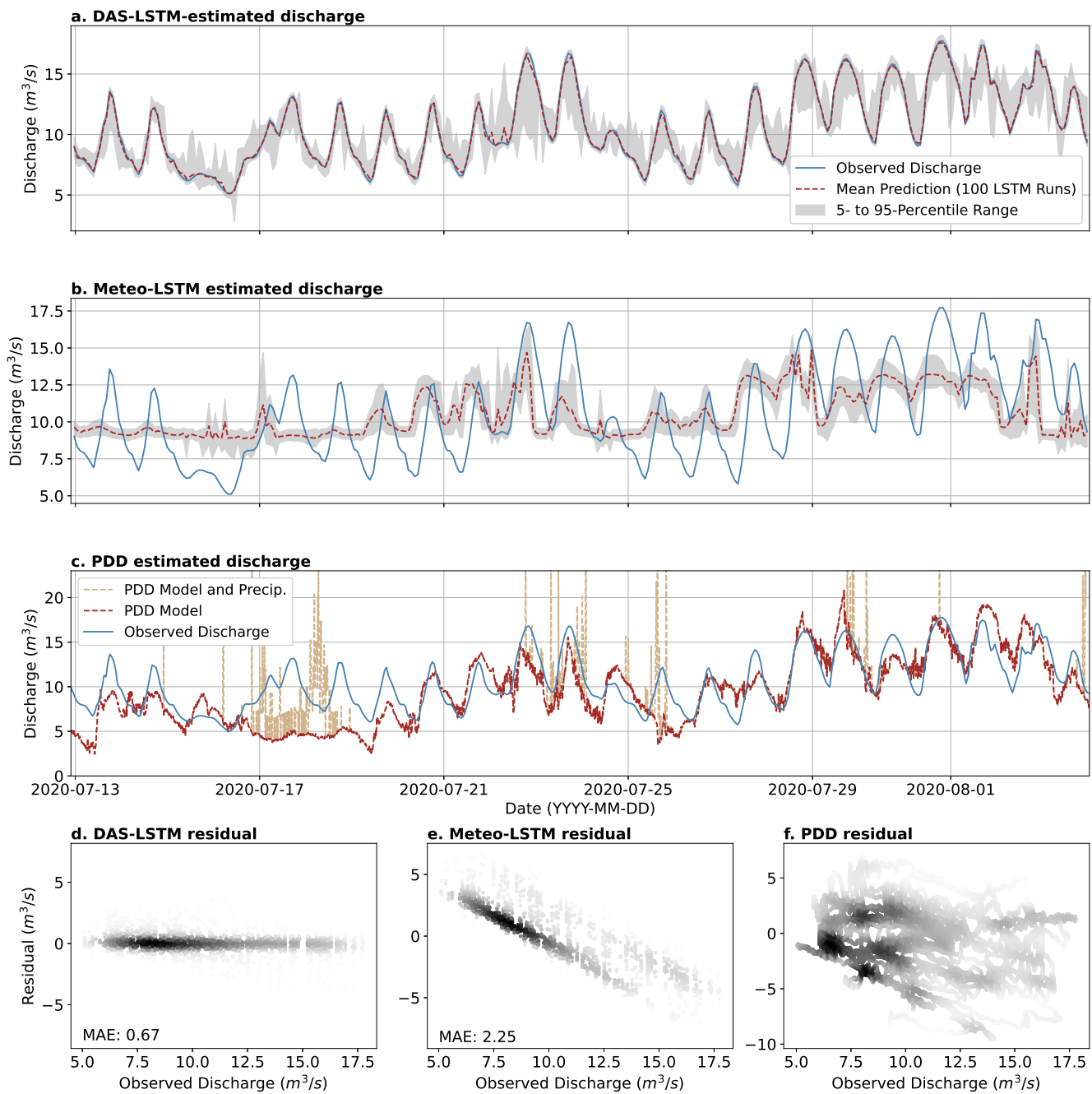


Fig. 3. a) DAS-LSTM model ensemble mean (red dashed) line and confidence interval (grey region) from cross validation (CV). b) same as a., but with the meteo-LSTM model. c) Positive degree day (PDD) model results. d-f) Residuals for the DAS-LSTM, Meteo-LSTM, and PDD models, respectively.

164 where z is the altitude, z_0 is the terminus altitude, D is the total predicted discharge, T is temperature,
165 γ is the calibrated lapse rate, f is the calibrated melt factor, P is the precipitation rate, and A is the
166 area of the glacier within each step in the summation. The glacier area is given as an idealized rectangle
167 with the glacier area, width, and elevation range as found in GLAMOS (GLAMOS and others, 2020). The
168 PDD model results were interpolated to match the times of discharge measurements used as LSTM model
169 targets. In order to compensate for meltwater transport from the proglacial lake to the discharge gauge
170 downstream, which is evident from the phase lag between a basic PDD model and measured discharge
171 curves, the PDD model results were shifted based on the phase of maximal cross correlation between
172 modeled and observed discharge.

173 RESULTS

174 The results of our analysis are listed in Table 1. For all of our analyses, we present results in terms of the
175 mean absolute error (MAE) of the residuals and the standard deviation of the residuals between model
176 outputs and discharge gauge measurements. All of these performance statistics are reported for the test
177 dataset in order to quantify model performance when evaluated on data that were not used for parameter
178 estimation. Overall, the best performing models use an LSTM architecture with input DAS data. These
179 models perform about 40% better than the NN model in terms of MAE. The LSTM models also result in
180 a more than 200 times reduction in mean absolute error compared to a linear model.

181 We plot the estimated discharge time series and residuals from our model (Figures 3a-c and d-f, respec-
182 tively). Examination of these time series confirms that the DAS-LSTM model is able to capture the phase
183 of discharge (Figure 3a). In contrast, the Meto-LSTM and PDD models, suffer from both poor amplitude
184 and phase response (Figure 3b and c).

185 Model residuals for the DAS-LSTM model show no systematic relationship with increasing discharge
186 (Figure 3d). The Meteo-LSTM model, in contrast, show both poor amplitude and phase response (Fig-
187 ure 3d) which is likely due to the poor correlation between temperature and precipitation amplitude and
188 phase. The PDD model estimates reasonable amplitudes with a phase shift. We therefore calculate PDD
189 residuals using a best fit time shift. Residuals for the PDD model are uncorrelated with increasing discharge
190 and an order of magnitude larger than the residuals from the DAS-LSTM model.

Table 1. Model types and mean absolute error (MAE) for test data set.

Model Type	Input Data	Data Processing	MAE (m ³ /s)	SD (m ³ /s)	Trainable parameters
Linear	DAS	50 Hz High-pass	145.41	232.76	461,601
NN	DAS	50 Hz High-pass	0.88	1.46	81,345
LSTM	DAS	50 Hz High-pass	0.67	1.18	299,681
LSTM	DAS	50 Hz Low-pass	0.68	1.25	299,681
LSTM	DAS	None	0.64	1.15	299,681
LSTM	Meteo	None	2.25	2.74	4,513
PDD	Meteo	None	2.72	3.26	0

191 Ablation zone versus accumulation zone

192 Models trained on ablation zone data performed better and have less variance than models that only used
 193 accumulation zone data. Models trained on data from the ablation zone have a mean MAE of 0.64 m³/s
 194 and standard deviation of 0.1 m³/s whereas models trained on accumulation zone data have a mean MAE
 195 of 1.07 m³/s and standard deviation of 0.24 m³/s. This can also be seen in the sensitivity analysis
 196 discussed in the Discussion section and shown in Figure 4 where particular sectors in the ablation zone
 197 generally show higher sensitivity to discharge than areas in the accumulation zone.

198 Meteo-LSTM and PDD results

199 The results of LSTM model runs with temperature and precipitation as inputs are shown in Figure 3b.
 200 The PDD predictions were shifted according to highest correlation coefficient, corresponding to 5.4 hours,
 201 before the residual was calculated to account for meltwater transport to the discharge gauge. The MAE of
 202 the residuals of the predictions on the test sets of data are 2.29 m³/s and 2.27 m³/s for the Meteo-LSTM
 203 and the PDD models, respectively.

204 Low-frequency versus high-frequency

205 Models trained on low frequency (<50 Hz) filtered DAS data perform slightly worse with a MAE of 0.68
 206 m³/s compared to 0.67 m³/s of the high frequency trained models while also having a larger residual
 207 standard deviation of 1.25 m³/s compared to 1.18 m³/s of highpass filtered models. An analysis of 100
 208 LSTM models trained on unfiltered DAS data was also done which performs slightly better than both

209 filtering methods with an MAE and standard deviation of 0.64 m³/s and 1.15 m³/s respectively which
210 may be explained by the broadband nature of the surficial hydrological soundscape (Podolskiy and others,
211 2023).

212 DISCUSSION

213 Our study demonstrates the potential for DAS-based glacio-hydrological sensing to be a robust technique
214 for potential in situ measurements of glacier runoff. We find good agreement with 0.64 m³/s MAE between
215 DAS-LSTM-inferred and stream gauge-measured discharge values. We begin this section by discussing
216 why the seismo-acoustic wavefield carries so much correlation with glacier discharge.

217 **The physical basis relating discharge to the seismo-acoustic wavefield**

218 As described in the Introduction, a wide variety of processes contribute to the glacier seismo-acoustic
219 wavefield. A key result that allows us to decipher the origin of our wavefield–discharge relationship is
220 that our regression analysis performs equally well or slightly better in the range 50-500 Hz as compared
221 to the range 0-50 Hz. This high frequency band eliminates the possibility that the dominant signal in our
222 analysis has its origin in subglacial processes such as conduit flow (Bartholomaus and others, 2015), gurgling
223 crevasses (Podolskiy, 2020), and bedload transport (Roth and others, 2016, 2017), all of which are thought
224 to create signal below 50 Hz. Furthermore, crevassing and basal stick-slip sliding is expected to generate
225 seismic signals above 50 Hz (Podolskiy and Walter, 2016) in addition to anthropogenic activity and wind
226 (Podolskiy and others, 2023) will also cause increased RMS. However, we infer that the sound generated
227 from supraglacial streams is the dominant contributor to our discharge regression analysis due to its
228 persistent existence during our melt-season measurement. Our basis for this inference is by comparison with
229 previous studies that have examined the the same acoustic frequency range in the context of terrestrial rivers
230 (Bolghasi and others, 2017; Osborne and others, 2021, 2022; Podolskiy and others, 2023). Additionally,
231 Figure S3 compares wind from the nearby meteo station to daily means of DAS strain rate and variance
232 RMS observations and show little correlation throughout the experiment which suggests that supraglacial
233 turbulent flow to be the dominant signal.

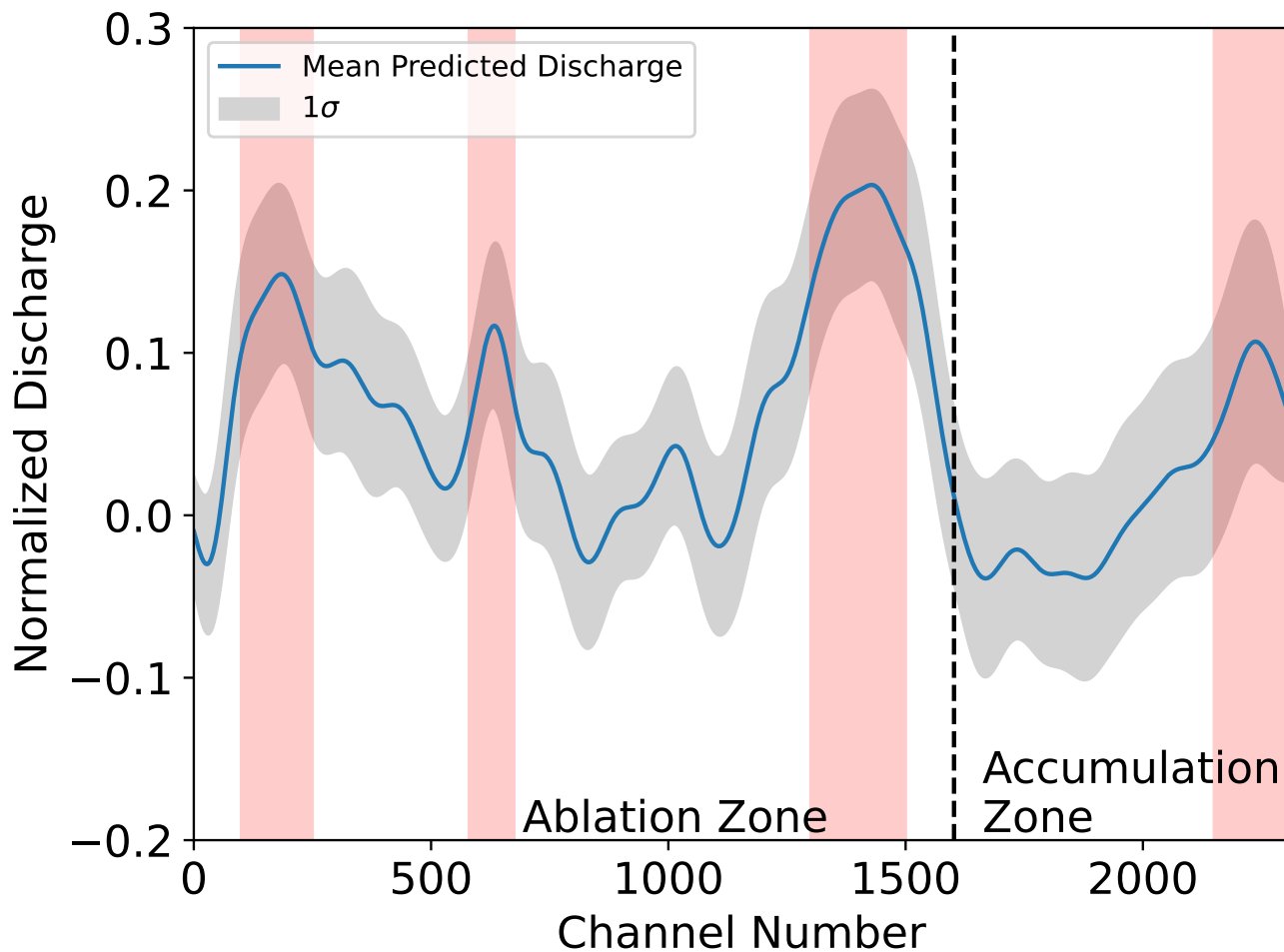


Fig. 4. Channel sensitivity analysis from applying a uniform in time Gaussian pulse with a width of 50 channels. A new discharge prediction is made each time the Gaussian pulse is centered on the next channel. The mean prediction is calculated from the predicted discharge of the 100 LSTM models produced. Predictions are given in values of a normalized discharge. A spatial trend in discharge sensitivity arises at four locations highlighted in red: three sectors in the ablation zone and one sector in the accumulation zone. At these locations, a given increase in normalized strain rate results in higher predicted normalized discharge values than would be expected at other locations along the cable. The dashed line denotes the approximate location of the transition from the ablation zone to the accumulation zone as determined by the drop in correlation of strain rate RMS with wind speed which reflects the cable melting into snow. This point had moved roughly a kilometer up glacier over the course of the experiment and may explain the significant peak in predicted discharge near the transition line.

234 **DAS offers a stable observation platform on melting glacier surfaces**

235 Ensuring the stability of instrumentation on the surface of glaciers is notoriously challenging (Carmichael,
236 2019). As a result, most seismic deployments in the ablation zone of glaciers, for example, only cover
237 spatial apertures on the order of 1 km (e.g. Rössli and others, 2014). Stream discharge in terrestrial
238 rivers is usually measured by establishing a relationship, called a rating curve, that empirically relates
239 stream height (also called stage) to discharge (Kennedy, 1984). In order to bypass logistical complexities
240 associated with this approach, recent studies have elected to pursue passive acoustic observation of river
241 height (Osborne and others, 2021; Podolskiy and others, 2023). The motivation to use seismo-acoustic
242 observations to study surficial glacier hydrology is even stronger given that seasonal variations in stream
243 morphology (Knighton, 1981; Marston, 1983; Karlstrom and others, 2013) would be expected to result
244 in a strongly time-dependent rating curve. For our study, the deployment of the cable along the glacier
245 flow line allows for sensitivity to source mechanisms in a wide area encompassing both the ablation and
246 accumulation zones. A particular benefit of fiber optic sensing over other methods is that the fiber optic
247 cable can be deployed strategically and is not limited to the specific instrumentation requirements such as
248 the availability of electrical power at the sensing location that hinder many other types of seismic sensing
249 equipment or other in situ instrumentation. In this study, the cable transects many features typical of
250 mountain glaciers: crevasses, supraglacial streams, rock debris, firn, snow, etc.

251 **Sensitivity Analysis**

252 All model iterations show a spatial sensitivity to predicting discharge. In Figure S2, we investigated
253 prediction performance relative to different parts of the cable by isolating the observed acoustic noise
254 in these locations. The DAS data was sectioned in three different ways and used as model input to
255 predict discharge: the whole cable, only channels within the ablation zone, and only channels within the
256 accumulation zone. We find model improvement when data within the ablation zone, where we expect the
257 most pervasive surface hydrology to exist, is used for training and prediction. When only the data from the
258 accumulation zone is used for training and prediction, the models perform markedly worse, 1.03 m³/s mean
259 MAE as compared to 0.63 m³/s mean MAE for the ablation data. In addition, the standard deviation
260 of the residuals is three times higher than that of the models using ablation data alone. In the following
261 subsections, we discuss possible mechanisms by which changes in the meltwater flow within supraglacial
262 streams as a result of temporal variation in discharge cause fluctuations in acoustic noise power as observed

263 by DAS.

264 Figure 4 shows a model sensitivity analysis where we generate a synthetic strain rate Gaussian pulse
265 with a width of 50 channels and uniform in time. The pulse is then centered on each channel before making
266 a discharge prediction. We iterate this procedure for each LSTM model trained on the whole cable DAS
267 data. Increased values of predicted normalized discharge for a given channel in Figure 4 indicate that an
268 increase of measured DAS strain rate or acoustic noise results in an increase of predicted discharge. Three
269 sectors of cable in the ablation zone centered around channel 150, 650, and 1400 are shown to be of more
270 importance to predicting discharge from DAS strain rate. Interestingly, a sector around channel 2250 in the
271 accumulation zone near the glacier headwall also imparts some sensitivity to predicted discharge. The most
272 sensitive portion of the cable is the sector around channel 1400 where the snow line is located during the
273 cable deployment time and the ice fall of Rhonegletscher is located. The melting of snow around the snow
274 line during the observation period caused the snow line to recede and exposed more bare ice to the fiber.
275 Surface crevassing, newly formed meltwater streams, and audible drainage from within exposed crevasses
276 may have all contributed to the high RMS strain rate signal in this area. This provides a first step into
277 the potential of forming a spatially-distributed, rather than integrated, inference of glacier surface melt.

278 **Transferable model to other glaciers**

279 We have shown that DAS can be used to infer glacier runoff on Rhonegletscher. Yet, it is worth noting
280 whether this method may be used on other glaciers to infer glacier discharge within their respective basins.
281 The geometry of the fiber deployment relative to surface flow has a significant impact on cable response,
282 thus the inference of discharge will vary. The channels weighted more significantly for discharge inference
283 may not be the same for every deployment or every catchment. Model retraining and testing will likely be
284 necessary to capture the multiple surface flow regimes during the summer melt and winter seasons. Glacier
285 catchments that have differing contributions of runoff and glacier melt to total discharge would require
286 further independent discharge measurements, at least initially, to validate the model inference. Despite
287 these initial limitations, the acoustic noise-discharge relationship appear to persist with a variety of flow
288 regimes (Podolskiy and others, 2023) which we expect to be the case supraglacially as well.

289 CONCLUSION

290 *In situ* measurements of glacier runoff have previously been logistically difficult to obtain, particularly in
291 areas with geographically complicated catchments or glaciers with distributed surface hydrological regimes.
292 We demonstrate a correlation between the *in situ* seismo-acoustic wavefield measured from the surface of a
293 glacier and proglacial discharge. Our machine learning model that relates these quantities identifies spatial
294 variability and coherence in discharge sensitivity to acoustics. The ability to quantify glacier runoff using
295 turbulent flow generated seismo-acoustics as observed by DAS opens the door to gaining insights into these
296 regions. Discharge predictions produced by DAS and ML could one day be ingested in glacier mass balance
297 models that have typically been limited by a lack of *in situ* glacier runoff validation (Lenaerts and others,
298 2019). In addition, seasonality of accumulation, ablation, and runoff may be characterized by changes in
299 acoustic signals that we observe here during the melt season; however, this will need to be investigated
300 in subsequent studies. Here, we have demonstrated the first of its kind application of DAS for inferring
301 glacier runoff.

302 REFERENCES

- 303 Bartholomaus TC, Amundson JM, Walter JJ, O'Neil S, West ME and Larsen CF (2015) Subglacial discharge at
304 tidewater glaciers revealed by seismic tremor. *Geophysical Research Letters*, **42**(15), 6391–6398, ISSN 1944-8007
305 (doi: 10.1002/2015GL064590), `_eprint: https://onlinelibrary.wiley.com/doi/pdf/10.1002/2015GL064590`
- 306 Bevan SL, Luckman AJ, Kuipers Munneke P, Hubbard B, Kulesa B and Ashmore DW (2018) Decline in surface
307 melt duration on Larsen C Ice Shelf revealed by the advanced scatterometer (ASCAT). *Earth and Space Science*,
308 **5**(10), 578–591, publisher: Wiley Online Library
- 309 Bishop CM and Nasrabadi NM (2006) *Pattern recognition and machine learning*, volume 4. Springer
- 310 Bolghasi A, Ghadimi P and Feizi Chekab MA (2017) Sound attenuation in air–water media with rough bubbly
311 interface at low frequencies considering bubble resonance dispersion. *Journal of the Brazilian Society of Mechanical*
312 *Sciences and Engineering*, **39**, 4859–4871, publisher: Springer
- 313 Booth AD, Christoffersen P, Pretorius A, Chapman J, Hubbard B, Smith EC, de Ridder S, Nowacki A, Lipovsky BP
314 and Denolle M (2023) Characterising sediment thickness beneath a Greenlandic outlet glacier using distributed

- 315 acoustic sensing: preliminary observations and progress towards an efficient machine learning approach. *Annals of*
316 *Glaciology*, 1–4, publisher: Cambridge University Press
- 317 Braithwaite RJ (1984) Calculation of degree-days for glacier-climate research. *Zeitschrift für Gletscherkunde und*
318 *Glazialgeologie*, **20**(1984), 1–8, publisher: Universitätsverlag Wagner
- 319 Braithwaite RJ (1995) Positive degree-day factors for ablation on the Greenland ice sheet studied by
320 energy-balance modelling. *Journal of Glaciology*, **41**(137), 153–160, ISSN 0022-1430, 1727-5652 (doi:
321 10.3189/S0022143000017846), publisher: Cambridge University Press
- 322 Burtin A, Bollinger L, Vergne J, Cattin R and Nábělek JL (2008) Spectral analysis of seismic noise in-
323 duced by rivers: A new tool to monitor spatiotemporal changes in stream hydrodynamics. *Journal*
324 *of Geophysical Research: Solid Earth*, **113**(B5), ISSN 2156-2202 (doi: 10.1029/2007JB005034), _eprint:
325 <https://onlinelibrary.wiley.com/doi/pdf/10.1029/2007JB005034>
- 326 Burtin A, Cattin R, Bollinger L, Vergne J, Steer P, Robert A, Findling N and Tiberi C (2011) Towards the hydrologic
327 and bed load monitoring from high-frequency seismic noise in a braided river: The “torrent de St Pierre”, French
328 Alps. *Journal of hydrology*, **408**(1-2), 43–53, publisher: Elsevier
- 329 Carmichael JD (2019) Narrowband signals recorded near a moulin that are not moulin tremor: a cautionary short
330 note. *Annals of Glaciology*, **60**(79), 231–237, ISSN 0260-3055, 1727-5644 (doi: 10.1017/aog.2019.23), publisher:
331 Cambridge University Press
- 332 Casassa G, López P, Pouyaud B and Escobar F (2009) Detection of changes in glacial run-off in alpine basins:
333 examples from North America, the Alps, central Asia and the Andes. *Hydrological Processes*, **23**(1), 31–41, ISSN
334 1099-1085 (doi: 10.1002/hyp.7194), _eprint: <https://onlinelibrary.wiley.com/doi/pdf/10.1002/hyp.7194>
- 335 Cauvy-Fraunié S, Andino P, Espinosa R, Calvez R, Jacobsen D and Dangles O (2016) Ecological responses to
336 experimental glacier-runoff reduction in alpine rivers. *Nature Communications*, **7**(1), 12025, ISSN 2041-1723 (doi:
337 10.1038/ncomms12025), number: 1 Publisher: Nature Publishing Group
- 338 Consortium G (2005) GLIMS Glacier Database, Version 1 (doi: 10.7265/N5V98602)
- 339 Cook KL, Andermann C, Gimbert F, Adhikari BR and Hovius N (2018) Glacial lake outburst floods as drivers of
340 fluvial erosion in the Himalaya. *Science*, **362**(6410), 53–57, publisher: American Association for the Advancement
341 of Science
- 342 Douglass AS, Abadi S and Lipovsky BP (2023) Distributed acoustic sensing for detecting near surface hydroacoustic
343 signals. *JASA Express Letters*, **3**(6) (doi: 10.1121/10.0019703), publisher: AIP Publishing

- 344 Fountain AG and Vecchia A (1999) How many stakes are required to measure the mass balance of a glacier? *Ge-*
345 *ografiska Annaler: Series A, Physical Geography*, **81**(4), 563–573, ISSN 0435-3676 (doi: 10.1111/1468-0459.00084),
346 publisher: Taylor & Francis _eprint: <https://www.tandfonline.com/doi/pdf/10.1111/1468-0459.00084>
- 347 Germain SLS and Moorman BJ (2019) Long-term observations of supraglacial streams on an Arctic glacier. *Journal*
348 *of Glaciology*, **65**(254), 900–911, ISSN 0022-1430, 1727-5652 (doi: 10.1017/jog.2019.60), publisher: Cambridge
349 University Press
- 350 Gimbert F, Tsai VC, Amundson JM, Bartholomaeus TC and Walter JI (2016) Subseasonal
351 changes observed in subglacial channel pressure, size, and sediment transport. *Geophysical Re-*
352 *search Letters*, **43**(8), 3786–3794, ISSN 1944-8007 (doi: 10.1002/2016GL068337), _eprint:
353 <https://agupubs.onlinelibrary.wiley.com/doi/pdf/10.1002/2016GL068337>
- 354 GLAMOS, Bauder A, Huss M and Linsbauer A (2020) *The Swiss Glaciers 2017/18 and 2018/19*, volume 139/140
355 of *Glaciological Report*. Cryospheric Commission (EKK) of the Swiss Academy of Sciences (SCNAT)
- 356 Haeberli W, Hoelzle M, Paul F and Zemp M (2007) Integrated monitoring of mountain glaciers as key indicators of
357 global climate change: the European Alps. *Annals of Glaciology*, **46**, 150–160, ISSN 0260-3055, 1727-5644 (doi:
358 10.3189/172756407782871512), publisher: Cambridge University Press
- 359 Hanna E, Huybrechts P, Janssens I, Cappelen J, Steffen K and Stephens A (2005) Runoff and mass balance of the
360 Greenland ice sheet: 1958–2003. *Journal of Geophysical Research: Atmospheres*, **110**(D13), ISSN 2156-2202 (doi:
361 10.1029/2004JD005641), _eprint: <https://onlinelibrary.wiley.com/doi/pdf/10.1029/2004JD005641>
- 362 Hock R (2005) Glacier melt: a review of processes and their modelling. *Progress in Physical Geography: Earth and*
363 *Environment*, **29**(3), 362–391, ISSN 0309-1333 (doi: 10.1191/0309133305pp453ra), publisher: SAGE Publications
364 Ltd
- 365 Hudson TS, Baird AF, Kendall JM, Kufner SK, Brisbourne AM, Smith AM, Butcher A, Chalari A and
366 Clarke A (2021) Distributed Acoustic Sensing (DAS) for Natural Microseismicity Studies: A Case Study
367 From Antarctica. *Journal of Geophysical Research: Solid Earth*, **126**(7), e2020JB021493, ISSN 2169-9356 (doi:
368 10.1029/2020JB021493), _eprint: <https://onlinelibrary.wiley.com/doi/pdf/10.1029/2020JB021493>
- 369 Huynh C, Hibert C, Jestin C, Malet J, Clément P and Lanticq V (2022) Real-Time Classification of Anthropogenic
370 Seismic Sources from Distributed Acoustic Sensing Data: Application for Pipeline Monitoring. *Seismological Re-*
371 *search Letters*, **93**(5), 2570–2583, ISSN 0895-0695 (doi: 10.1785/0220220078)
- 372 Karlstrom L, Gajjar P and Manga M (2013) Meander formation in supraglacial streams. *Journal of Geophysical*
373 *Research: Earth Surface*, **118**(3), 1897–1907, publisher: Wiley Online Library

- 374 Kennedy EJ (1984) *Discharge ratings at gaging stations*. Department of the Interior, US Geological Survey
- 375 Klaasen S, Paitz P, Lindner N, Dettmer J and Fichtner A (2021) Distributed Acoustic Sensing in Volcano-Glacial
376 Environments—Mount Meager, British Columbia. *Journal of Geophysical Research: Solid Earth*, **126**(11), ISSN
377 2169-9313, 2169-9356 (doi: 10.1029/2021JB022358)
- 378 Knighton AD (1981) Channel Form and Flow Characteristics of Supraglacial Streams, Austre Okstindbreen, Nor-
379 way. *Arctic and Alpine Research*, **13**(3), 295–306, ISSN 0004-0851 (doi: 10.2307/1551036), publisher: INSTAAR,
380 University of Colorado
- 381 Landmann JM (2022) Near-Real-Time Monitoring, Modelling, and Data Assimilation of Glacier Mass Balance. *VAW-*
382 *Mitteilungen*, **269**, accepted: 2022-08-09T06:31:28Z Publisher: Eigenverlag der Versuchsanstalt für Wasserbau,
383 Hydrologie und Glaziologie (VAW), ETH Zürich
- 384 Landmann JM, Künsch HR, Huss M, Ogier C, Kalisch M and Farinotti D (2021) Assimilating near-real-time mass
385 balance stake readings into a model ensemble using a particle filter. *The Cryosphere*, **15**(11), 5017–5040, ISSN
386 1994-0416 (doi: 10.5194/tc-15-5017-2021), publisher: Copernicus GmbH
- 387 Lenaerts JTM, Medley B, van den Broeke MR and Wouters B (2019) Observing and Modeling Ice Sheet Surface
388 Mass Balance. *Reviews of Geophysics*, **57**(2), 376–420, ISSN 1944-9208 (doi: 10.1029/2018RG000622), _eprint:
389 <https://onlinelibrary.wiley.com/doi/pdf/10.1029/2018RG000622>
- 390 Lindsey NJ and Martin ER (2021) Fiber-optic seismology. *Annual Review of Earth and Planetary Sciences*, **49**,
391 309–336, publisher: Annual Reviews
- 392 Linsbauer A, Paul F, Machguth H and Haeberli W (2013) Comparing three different methods to model scenarios of
393 future glacier change in the Swiss Alps. *Annals of Glaciology*, **54**(63), 241–253, ISSN 0260-3055, 1727-5644 (doi:
394 10.3189/2013AoG63A400), publisher: Cambridge University Press
- 395 Manasseh R, Babanin AV, Forbes C, Rickards K, Bobevski I and Ooi A (2006) Passive acoustic determination of
396 wave-breaking events and their severity across the spectrum. *Journal of Atmospheric and Oceanic Technology*,
397 **23**(4), 599–618, publisher: American Meteorological Society
- 398 Mark BG and Seltzer GO (2003) Tropical glacier meltwater contribution to stream discharge: a case study
399 in the Cordillera Blanca, Peru. *Journal of Glaciology*, **49**(165), 271–281, ISSN 0022-1430, 1727-5652 (doi:
400 10.3189/172756503781830746), publisher: Cambridge University Press
- 401 Markus T, Neumann T, Martino A, Abdalati W, Brunt K, Csatho B, Farrell S, Fricker H, Gardner A, Harding D,
402 Jasinski M, Kwok R, Magruder L, Lubin D, Luthcke S, Morison J, Nelson R, Neuenschwander A, Palm S, Popescu
403 S, Shum C, Schutz BE, Smith B, Yang Y and Zwally J (2017) The Ice, Cloud, and land Elevation Satellite-2

- 404 (ICESat-2): Science requirements, concept, and implementation. *Remote Sensing of Environment*, **190**, 260–273,
405 ISSN 0034-4257 (doi: 10.1016/j.rse.2016.12.029)
- 406 Marston RA (1983) Supraglacial Stream Dynamics on the Juneau Icefield. *Annals of the Association of*
407 *American Geographers*, **73**(4), 597–608, ISSN 1467-8306 (doi: 10.1111/j.1467-8306.1983.tb01861.x), __eprint:
408 <https://onlinelibrary.wiley.com/doi/pdf/10.1111/j.1467-8306.1983.tb01861.x>
- 409 Martín Abadi, Ashish Agarwal, Paul Barham, Eugene Brevdo, Zhifeng Chen, Craig Citro, Greg S Corrado, Andy
410 Davis, Jeffrey Dean, Matthieu Devin, Sanjay Ghemawat, Ian Goodfellow, Andrew Harp, Geoffrey Irving, Michael
411 Isard, Jia Y, Rafal Jozefowicz, Lukasz Kaiser, Manjunath Kudlur, Josh Levenberg, Dandelion Mané, Rajat Monga,
412 Sherry Moore, Derek Murray, Chris Olah, Mike Schuster, Jonathon Shlens, Benoit Steiner, Ilya Sutskever, Kunal
413 Talwar, Paul Tucker, Vincent Vanhoucke, Vijay Vasudevan, Fernanda Viégas, Oriol Vinyals, Pete Warden, Martin
414 Wattenberg, Martin Wicke, Yuan Yu and Xiaoqiang Zheng (2015) TensorFlow: Large-Scale Machine Learning on
415 Heterogeneous Systems
- 416 Morse N, Bowden WB, Hackman A, Pruden C, Steiner E and Berger E (2007) Using sound pressure to estimate
417 reaeration in streams. *Journal of the North American Benthological Society*, **26**(1), 28–37
- 418 Nanni U, Gimbert F, Vincent C, Gräff D, Walter F, Piard L and Moreau L (2020) Quantification of seasonal and
419 diurnal dynamics of subglacial channels using seismic observations on an Alpine glacier. *The Cryosphere*, **14**(5),
420 1475–1496, ISSN 1994-0416 (doi: 10.5194/tc-14-1475-2020), publisher: Copernicus GmbH
- 421 Nicholson L, Wirbel A, Mayer C and Lambrecht A (2021) The Challenge of Non-Stationary Feedbacks in Modeling
422 the Response of Debris-Covered Glaciers to Climate Forcing. *Frontiers in Earth Science*, **9**, ISSN 2296-6463
- 423 Osborne WA, Hodge RA, Love GD, Hawkin P and Hawkin RE (2021) Babbling brook to thunderous torrent: Using
424 sound to monitor river stage. *Earth Surface Processes and Landforms*, **46**(13), 2656–2670, publisher: Wiley Online
425 Library
- 426 Osborne WA, Hodge RA, Love GD, Hawkin P and Hawkin RE (2022) The Influence of In-Channel Obstacles on
427 River Sound. *Water Resources Research*, **58**(4), e2021WR031567, ISSN 1944-7973 (doi: 10.1029/2021WR031567),
428 __eprint: <https://onlinelibrary.wiley.com/doi/pdf/10.1029/2021WR031567>
- 429 Podolskiy EA (2020) Toward the acoustic detection of two-phase flow patterns and Helmholtz resonators in englacial
430 drainage systems. *Geophysical Research Letters*, **47**(6), e2020GL086951
- 431 Podolskiy EA and Walter F (2016) Cryoseismology. *Reviews of Geophysics*, **54**(4), 708–758, ISSN 1944-9208 (doi:
432 10.1002/2016RG000526), __eprint: <https://onlinelibrary.wiley.com/doi/pdf/10.1002/2016RG000526>

- 433 Podolskiy EA, Imazu T and Sugiyama S (2023) Acoustic Sensing of Glacial Discharge in Greenland. *Geophysical*
434 *Research Letters*, **50**(8), e2023GL103235, ISSN 0094-8276, 1944-8007 (doi: 10.1029/2023GL103235)
- 435 Pratap B, Dobhal DP, Mehta M and Bhambri R (2015) Influence of debris cover and altitude on glacier surface
436 melting: a case study on Dokriani Glacier, central Himalaya, India. *Annals of Glaciology*, **56**(70), 9–16, ISSN
437 0260-3055, 1727-5644 (doi: 10.3189/2015AoG70A971), publisher: Cambridge University Press
- 438 Prosperetti A (1988) Bubble-related ambient noise in the ocean. *The Journal of the Acoustical Society of America*,
439 **84**(3), 1042–1054, publisher: Acoustical Society of America
- 440 Ridley J (1993) Surface melting on Antarctic Peninsula ice shelves detected by passive microwave sensors. *Geophysical*
441 *Research Letters*, **20**(23), 2639–2642, publisher: Wiley Online Library
- 442 Ronan TJ, Lees JM, Mikesell TD, Anderson JF and Johnson JB (2017) Acoustic and Seismic Fields of Hydraulic
443 Jumps at Varying Froude Numbers. *Geophysical Research Letters*, **44**(19), 9734–9741, ISSN 1944-8007 (doi:
444 10.1002/2017GL074511), _eprint: <https://onlinelibrary.wiley.com/doi/pdf/10.1002/2017GL074511>
- 445 Roth DL, Brodsky EE, Finnegan NJ, Rickenmann D, Turowski JM and Badoux A (2016) Bed load sediment transport
446 inferred from seismic signals near a river. *Journal of Geophysical Research: Earth Surface*, **121**(4), 725–747, ISSN
447 2169-9011 (doi: 10.1002/2015JF003782), _eprint: <https://onlinelibrary.wiley.com/doi/pdf/10.1002/2015JF003782>
- 448 Roth DL, Finnegan NJ, Brodsky EE, Rickenmann D, Turowski JM, Badoux A and Gimbert F (2017) Bed load
449 transport and boundary roughness changes as competing causes of hysteresis in the relationship between river
450 discharge and seismic amplitude recorded near a steep mountain stream. *Journal of Geophysical Research: Earth*
451 *Surface*, **122**(5), 1182–1200, publisher: Wiley Online Library
- 452 Rösli C, Walter F, Husen S, Andrews LC, Lüthi MP, Catania GA and Kissling E (2014) Sustained seismic tremors
453 and icequakes detected in the ablation zone of the Greenland ice sheet. *Journal of Glaciology*, **60**(221), 563–575,
454 publisher: Cambridge University Press
- 455 Schaeffli B, Manso P, Fischer M, Huss M and Farinotti D (2019) The role of glacier retreat for Swiss hydropower
456 production. *Renewable Energy*, **132**, 615–627, ISSN 0960-1481 (doi: 10.1016/j.renene.2018.07.104)
- 457 Schmandt B, Aster RC, Scherler D, Tsai VC and Karlstrom K (2013) Multiple fluvial processes de-
458 tected by riverside seismic and infrasound monitoring of a controlled flood in the Grand Canyon.
459 *Geophysical Research Letters*, **40**(18), 4858–4863, ISSN 1944-8007 (doi: 10.1002/grl.50953), _eprint:
460 <https://onlinelibrary.wiley.com/doi/pdf/10.1002/grl.50953>
- 461 Shatalin S, Parker T and Farhadiroushan M (2021) High definition seismic and microseismic data acquisition using
462 distributed and engineered fiber optic acoustic sensors. *Distributed acoustic sensing in geophysics: Methods and*
463 *applications*, 1–32, publisher: Wiley Online Library

- 464 Shreve RL (1972) Movement of Water in Glaciers*. *Journal of Glaciology*, **11**(62), 205–214, ISSN 0022-1430, 1727-
465 5652 (doi: 10.3189/S002214300002219X), publisher: Cambridge University Press
- 466 Sutterley TC, Velicogna I, Fettweis X, Rignot E, Noël B and van den Broeke M (2018) Evaluation of reconstructions
467 of snow/ice melt in Greenland by regional atmospheric climate models using laser altimetry data. *Geophysical*
468 *Research Letters*, **45**(16), 8324–8333, publisher: Wiley Online Library
- 469 Titov A, Fan Y, Kutun K and Jin G (2022) Distributed Acoustic Sensing (DAS) Response of Rising Taylor Bubbles in
470 Slug Flow. *Sensors*, **22**(3), 1266, ISSN 1424-8220 (doi: 10.3390/s22031266), number: 3 Publisher: Multidisciplinary
471 Digital Publishing Institute
- 472 Trusel LD, Frey KE, Das SB, Munneke PK and van den Broeke MR (2013) Satellite-based estimates of
473 Antarctic surface meltwater fluxes. *Geophysical Research Letters*, **40**(23), 6148–6153, ISSN 1944-8007 (doi:
474 10.1002/2013GL058138), __eprint: <https://onlinelibrary.wiley.com/doi/pdf/10.1002/2013GL058138>
- 475 Vahabi N, Willman E, Baghsiahi H and Selviah DR (2020) Fluid Flow Velocity Measurement in Active Wells Using
476 Fiber Optic Distributed Acoustic Sensors. *IEEE Sensors Journal*, **20**(19), 11499–11507, ISSN 1558-1748 (doi:
477 10.1109/JSEN.2020.2996823), conference Name: IEEE Sensors Journal
- 478 Walter F, Gräff D, Lindner F, Paitz P, Köpfl M, Chmiel M and Fichtner A (2020) Distributed acoustic sensing of
479 microseismic sources and wave propagation in glaciated terrain. *Nature Communications*, **11**(1), 2436, ISSN 2041-
480 1723 (doi: 10.1038/s41467-020-15824-6), bandiera_abtest: a Cc_license_type: cc_by Cg_type: Nature Research
481 Journals Number: 1 Primary_atype: Research Publisher: Nature Publishing Group Subject_term: Cryospheric
482 science;Natural hazards;Seismology Subject_term_id: cryospheric-science;natural-hazards;seismology
- 483 Wille JD, Favier V, Dufour A, Gorodetskaya IV, Turner J, Agosta C and Codron F (2019) West Antarctic surface
484 melt triggered by atmospheric rivers. *Nature Geoscience*, **12**(11), 911–916, publisher: Nature Publishing Group
485 UK London
- 486 Wouters B, Chambers D and Schrama E (2008) GRACE observes small-scale mass loss in Greenland. *Geophysical*
487 *Research Letters*, **35**(20), publisher: Wiley Online Library
- 488 Yang K and Li M (2014) Greenland Ice Sheet surface melt: A review. *Sciences in Cold and Arid Regions*, **6**, 0099–0106
489 (doi: 10.3724/SP.J.1226.2014.00099)
- 490 Yang K and Smith LC (2013) Supraglacial Streams on the Greenland Ice Sheet Delineated From Combined Spec-
491 tral–Shape Information in High-Resolution Satellite Imagery. *IEEE Geoscience and Remote Sensing Letters*, **10**(4),
492 801–805, ISSN 1558-0571 (doi: 10.1109/LGRS.2012.2224316), conference Name: IEEE Geoscience and Remote
493 Sensing Letters

494 Zekollari H, Huss M and Farinotti D (2019) Modelling the future evolution of glaciers in the European Alps under
495 the EURO-CORDEX RCM ensemble. *The Cryosphere*, **13**(4), 1125–1146, ISSN 1994-0416 (doi: 10.5194/tc-13-
496 1125-2019), publisher: Copernicus GmbH

For Peer Review

Supporting Information for "DAS to Discharge: Using Distributed Acoustic Sensing (DAS) to infer glacier runoff"

John-Morgan MANOS¹, Dominik GRÄFF¹, Eileen R. MARTIN², Patrick PAITZ³, Fabian WALTER⁴, Andreas FICHTNER³, Bradley P. LIPOVSKY¹

¹*Department of Earth and Space Sciences, University of Washington, Seattle, WA, USA*

²*Department of Geophysics and Department of Applied Math and Statistics, Colorado School of Mines, Golden, CO, USA*

³*ETH Zurich, Department of Earth Sciences, Institute of Geophysics, Zurich, Switzerland*

⁴*Swiss Federal Institute for Forest, Snow and Landscape Research WSL, Zürich, Switzerland*

Correspondence: John-Morgan Manos <jmanos@uw.edu>

Contents of this file

1. Figure S1 to S3

Introduction Here, we provide supplemental figures which describe the method for model and window size selection, and an analysis on the relative prediction performance using only certain parts of the cable. In addition, we further elaborate on the hyperparameter tuning procedure used to create the machine learning models used for discharge prediction.

Hyperparameter tuning.

Figure 1 shows the hyperparameter tuning of model input window sizes and a comparison between model types. The window sizes correspond to the number of 30 second timesteps to include in the window for model training, validation, and testing. For example, a window size of 20 corresponds to a window size of 10 minutes time by number of channels. The linear machine learning model used for comparison performs an order of magnitude worse in all tested window sizes. The Long Short-Term Memory (LSTM) model and Neural Network (NN) models perform similarly; however, LSTM tends to be the better performing model with less variance over most of the tested window sizes hence our selection for further testing. Models with large window sizes (>500) tend to break down in their predictive precision and accuracy as the number of training batches is reduced. Models with small window sizes (<20) tend to perform significantly better and have lower variance which may be explained by the increase in training batches and that the discharge

28 value is relatively stable at sufficiently small timescales. To combat these artifacts that misrepresent the
29 power of machine learning inference of discharge, we opted to choose a window size sufficiently large enough
30 to capture the meltwater transport down stream to the discharge gauge which we chose as a window size
31 of 200 corresponding to 100 minutes of data. A learning rate of 0.001 was chosen for the analysis as we
32 found varying the learning rate slightly did not change results significantly and a learning rate of 0.001 is
33 fairly standard in machine learning applications.

34 **Data shuffling and splitting for model ingest.** To include all possible surface melt regimes encountered
35 during the observation period in our analysis, we performed 100 iterations of data windowing, shuffling,
36 model creation, and batching into training, validation, and testing data sets. The ratio of training, valida-
37 tion, and test data set size was kept fixed between each iteration at 70, 20, and 10 percent, respectively.
38 The windows are non-overlapping and the data sets split into training, validation, and test sets are com-
39 pletely separate from each other for each iteration. Depending on the batch size, which was kept at 32 for
40 the study but allowed to vary during the window size testing phase, the test set would contain inconsistent
41 batch sizes. In these cases, the final batch created from the remainder timesteps would be removed from
42 the test data set as to keep consistent batch sizes for model ingest and prediction.

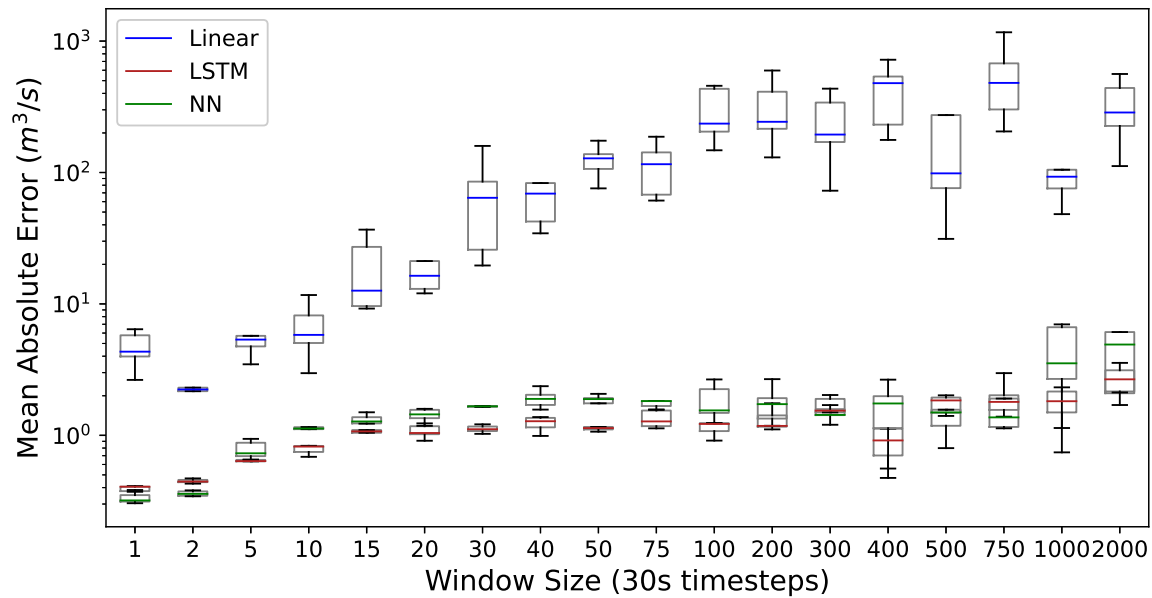


Fig. S 1. (Supplemental) Mean absolute error (MAE) from 18 window size hyperparameterizations tested with three different types of machine learning model architectures: Linear, LSTM, and NN. The box signifies the interquartile range and the whiskers are the last data point in the range that are less than 1.5 times the interquartile range. A linear machine learning framework performs significantly worse than the LSTM and NN architectures. LSTM and NN architectures perform comparably well, however, the LSTM achieves better performance at a wider range of window sizes.

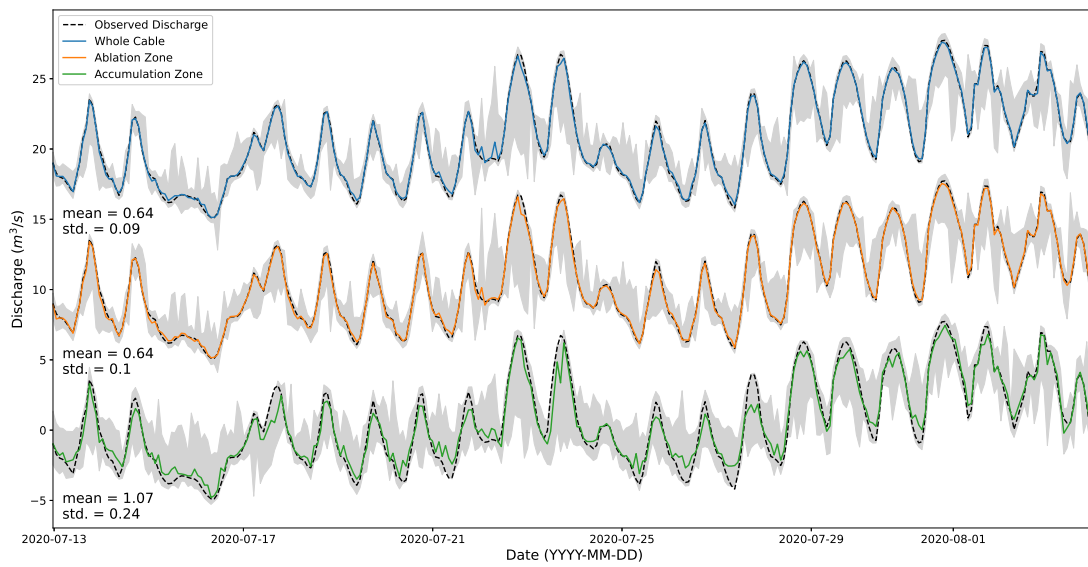


Fig. S 2. (Supplemental) Model performance from 100 model runs for models trained on all data (top, blue), data taken only from the section of cable in the ablation zone as determined to be from channels 0 - 1602 (middle, orange), and data taken only from the section of cable in the accumulation zone as determined to be channels numbered higher than 1602 (bottom, green). The mean and standard deviation (std) is calculated for the mean absolute error for each of the 100 model run sets and reported below the respective predictions on the sectioned data sets. Note that the blue and green curves are systematically offset from each other along the y-axis by $\pm 10m^3/s$ for comparison purposes.

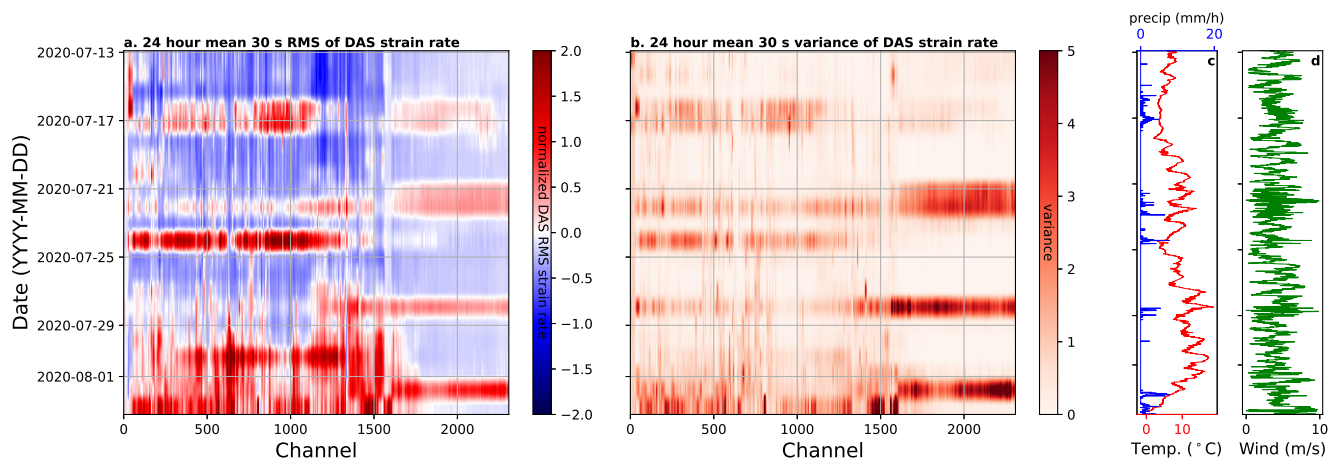


Fig. S 3. (Supplemental) **a)** Mean of normalized 30 s RMS strain rate over 24 hour periods with respect to channel. **b)** Variance of normalized 30 s RMS strain rate over 24 hour periods. **c)** Hourly temperature, precipitation, and **d)** wind data from 10 min recordings at Grimsel Hospitz meteo station (Swiss Federal Office of Meteorology and Climatology MeteoSwiss).